Monthly Notices
of the
ROYAL ASTRONOMICAL SOCIETY

MNRAS **472,** 3554–3563 (2017) doi:10.1093/mnras/stx2090

The multi-line slope method for measuring the effective magnetic field of cool stars: an application to the solar-like cycle of ϵ Eri

C. Scalia,[1,2]★ F. Leone,[1,2]★ M. Gangi,[1,2]★ M. Giarrusso[1,2] and M. J. Stift[3]

[1]*Università di Catania, Dipartimento di Fisica e Astronomia, Sezione Astrofisica, Via S. Sofia 78, I–95123 Catania, Italy*
[2]*INAF – Osservatorio Astrofisico di Catania, Via S. Sofia 78, I–95123 Catania, Italy*
[3]*Armagh Observatory, College Hill, Armagh BT61 9DG, Northern Ireland, UK*

Accepted 2017 August 10. Received 2017 August 10; in original form 2017 May 16

ABSTRACT

One method for the determination of integrated longitudinal stellar fields from low-resolution spectra is the so-called *slope method*, which is based on the regression of the Stokes *V* signal against the first derivative of Stokes *I*. Here we investigate the possibility of extending this technique to measure the magnetic fields of cool stars from high-resolution spectra. For this purpose we developed a multi-line modification to the slope method, called the *multi-line slope method*. We tested this technique by analysing synthetic spectra computed with the COSSAM code and real observations obtained with the high-resolution spectropolarimeters Narval, HARPSpol and the Catania Astrophysical Observatory Spectropolarimeter (CAOS). We show that the multi-line slope method is a fast alternative to the least squares deconvolution technique for the measurement of the effective magnetic fields of cool stars. Using a Fourier transform on the effective magnetic field variations of the star ϵ Eri, we find that the long-term periodicity of the field corresponds to the 2.95-yr period of the stellar dynamo, revealed by the variation of the activity index.

Key words: polarization – stars: late-type – stars: magnetic field.

1 INTRODUCTION

Magnetic fields are among the most important, yet most elusive, physical phenomena affecting the physics of the atmosphere of late-type stars. Direct observation of them is difficult because their effects are usually hidden in the typical noise of astronomical observations.

In this context, indicators of stellar magnetism are chromospheric Ca lines (Schrijver et al. 1989) and coronal X-ray emission (Pevtsov et al. 2003); however, neither of these is directly related to the field strength. As reported by Judge & Thompson (2012), an empirical correlation between Zeeman signals of the magnetic field and chromospheric indices has been found in the Sun and in other stars, such as ξ Boo (Morgenthaler et al. 2010).

Measuring and monitoring the behaviour of the magnetic field of late-type stars is important in order to gain a better understanding of dynamo theories. It is widely accepted that the physical processes involved in the origin of the magnetic field in cool stars are the same as in the Sun, but with a different set of parameters, such as temperature, gravity and stellar rotation (Reiners 2012). The magnetic field is an essential ingredient in chromospheric and coronal heating. It also plays a role in the accretion of circumstellar material onto the stellar surface (Bouvier et al. 2007), in the theory of the formation of exoplanets, and in star–planet interaction (Preusse et al. 2006; Strugarek et al. 2015). The impact of magnetic fields alters the stellar activity can mimic the modulation of the stellar radial velocity caused by the presence of exoplanets (Dumusque et al. 2012), leading to false detections (Queloz et al. 2001), for example the planetary systems of HD 219542 (Desidera et al. 2004), HD 200466 (Carolo et al. 2014) and HD 99492 (Kane et al. 2016).

The polarization signal resulting from the Zeeman effect is so small in cool stars that the current instrumentation is not able to detect it in individual spectral lines. For this reason, several techniques are being developed to enable the detection of magnetic signals. Semel & Li (1996) proposed a multi-line technique that combines the polarization signal originating from several spectral lines into one pseudo-profile, with a higher signal-to-noise ratio. The most frequently used method to add spectral profiles is least squares deconvolution (LSD) (Donati et al. 1997). There are other techniques, however, such as principal component analysis (Semel et al. 2009) or Zeeman component decomposition (Sennhauser & Berdyugina 2010).

In this paper we present an alternative method to measure the integrated longitudinal magnetic field strength of cool stars. We extend to high-resolution spectroscopy the method applied by Bagnulo et al. (2002) to low-resolution spectra. Our technique, hereafter called the multi-line slope method, allows us to measure the

★ E-mail: cscalia@oact.inaf.it (CS); fleone@oact.inaf.it (FL); mgi@oact.inaf.it (MG)

field from the slope of Stokes V versus the spectral derivative of Stokes I. We apply the multi-line slope method to high-resolution data from the K2V star ϵ Eri. We analyse data from archives of NARVAL (Aurière 2003) and HARPSpol (Snik et al. 2011; Piskunov et al. 2011) and from new observations obtained with the spectropolarimeter CAOS (Leone et al. 2016).

The paper is organized as follow. In Section 2 we describe the data set of observations of ϵ Eri. In Section 3 we describe the general slope method, and in Section 4 we introduce the multi-line approach and subsequently test it numerically. Section 5 presents a comparison of the multi-line slope method with the LSD technique. In Section 6 we discuss the measurements of the magnetic field of ϵ Eri, and in Section 7 we report the final conclusions of the work.

2 OBSERVATIONS

2.1 CAOS

We started to observe the star ϵ Eri using the Catania Astrophysical Observatory Spectropolarimeter (CAOS) in 2014. The instrument is fibre-linked to the 0.91-m telescope of the Catania Astrophysical Observatory (G. M. Fracastoro Stellar Station, Serra La Nave, Mt Etna, Italy).

Stokes V observations are recorded through a Savart plate and a $\lambda/4$ wave-plate, with exposures at angles of 45° and 135°. Following Tinbergen & Rutten (1992), single exposures of a polarimeter are affected by two functions, G and $F(t)$, which are time-independent and time-dependent, respectively:

$$i_{\rm o} = 0.5\,(I+V)\,G_{\rm o}\,F(t); \quad i_{\rm s} = 0.5\,(I-V)\,G_{\rm s}\,F(t). \tag{1}$$

From the ratios of the single exposures:

$$R_V^4 = \frac{i_{1\rm o}}{i_{2\rm o}}\frac{i_{2\rm s}}{i_{1\rm s}}\frac{i_{4\rm o}}{i_{3\rm o}}\frac{i_{3\rm s}}{i_{4\rm s}}; \quad R_N^4 = \frac{i_{1\rm o}}{i_{2\rm o}}\frac{i_{2\rm s}}{i_{1\rm s}}\frac{i_{3\rm o}}{i_{4o}}\frac{i_{4\rm s}}{i_{3\rm s}}. \tag{2}$$

We computed Stokes V and the null profile (Donati et al. 1997):

$$\frac{V}{I} = \frac{R_V-1}{R_V+1}; \quad \frac{N}{I} = \frac{R_N-1}{R_N+1}. \tag{3}$$

The stability of the wavelength calibration in time is of crucial importance for the combination of the exposures. We calibrated a thorium–argon reference lamp to a precision of 10^{-4} Å. In order to achieve high-accuracy measurements, we paid particular attention to the thermal stability of the spectrograph, which is better than 0.01 K.

2.2 Data from archives

In this work we use all the available spectropolarimetric observations of ϵ Eri. The archival data consist of HARPSpol and NARVAL observations. HARPSpol is located on the 3.6-m telescope in La Silla, while Narval is located on the 2.2-m Telescope Bernard Lyot.

The raw science and the calibration files of the HARPSpol observations were downloaded from the ESO archive[1] and they refer to observations taken in 2010 January and 2011 February. We performed the data reduction using IRAF packages and computed Stokes V through equations (2) and (3).

NARVAL data were downloaded from the PolarBase data base[2] (Petit et al. 2014) and refer to six distinct epochs: 2007 January, 2008 January, 2010 January, 2011 October, 2012 October and 2013 October.

The complete logbook of the observations is given in Table 5.

[1] http://archive.eso.org/eso/eso_archive_main.html
[2] http://polarbase.irap.omp.eu/

3 THE SLOPE METHOD

The slope method is based on the assumption of the weak-field approximation. If we assume that the Zeeman pattern can be approximated by a classical triplet, and if the Zeeman separation $\Delta\lambda_B$ is small compared with the intrinsic broadening of a spectral line, then the emergent circular polarization from a point on the surface of a star can be written as a function of the spectral derivative of Stokes I (Unno 1956):

$$V(\lambda,\theta) = \Delta\lambda_B\,\cos\phi\,\frac{{\rm d}I(\lambda,\theta)}{{\rm d}\lambda}, \tag{4}$$

where ϕ and θ are respectively the angle between the magnetic field vector and the line of sight, and the angle between the local surface normal and the line of sight, and the Zeeman separation is given by

$$\Delta\lambda_B = 4.67\times10^{-13}\,g_{\rm eff}\,\lambda^2\,B, \tag{5}$$

where $g_{\rm eff}$ is the effective Landé factor, B is the field strength expressed in gauss, and λ is the wavelength in angstrom.

The previous equation (4) is strictly valid for a single element of the stellar surface. Landstreet (1982) noted that the extension to the stellar (spatially unresolved) case runs into difficulties (1) related to stellar rotation, which Doppler shifts the local profiles, and (2) because both $\Delta\lambda_B$ and the angle ϕ vary over the visible stellar disc. Assuming that the velocity broadening is small compared with the intrinsic (magnetic) broadening, he showed that the observed Stokes V is related to the observed Stokes I as

$$\frac{V}{I} = -4.67\times10^{-13}\,g_{\rm eff}\,\lambda^2 B_{\rm eff}\,\frac{{\rm d}I}{{\rm d}\lambda}\,\frac{1}{I}, \tag{6}$$

where $B_{\rm eff}$ is the integral over the visible hemisphere of the magnetic field component along the line of sight, usually called the effective magnetic field, expressed in gauss.

Bagnulo et al. (2002) introduced the idea of measuring the effective magnetic field of faint stars through the application of equation (6) to low-resolution ($R \leq 5000$) spectra. However, this equation holds if line profiles are shaped by the magnetic field and not by the instrumental broadening. This condition means that the method suggested by Bagnulo and co-workers was well suited for early-type stars, whose Balmer lines dominate at low resolution. For example, Kolenberg & Bagnulo (2009) found no evidence of magnetic fields in RR Lyrae stars, Leone (2007) observed some magnetic A-type stars to test the capability of the William Hershel Telescope to measure the stellar magnetic field, Leone et al. (2011) gave an upper limit for the magnetic field in the central stars of planetary nebulae, and Hubrig et al. (2016) detected magnetic fields in Wolf–Rayet stars.

4 THE MULTI-LINE SLOPE METHOD

Equation (6) holds for any spectral line shaped by the magnetic field, and, in principle, simultaneous application to a large number of spectral lines can result in a very sensitive measurement of the field, as is the case for radial velocities, for which thousands of spectral lines result in a cross-correlation function.

Bagnulo et al. (2002) pointed out that equation (6) is restricted to unblended lines, so that the method cannot be applied to metal lines as observed in low-resolution spectroscopy. We propose an

extension of the slope method to the unblended lines of late-type stars observed at high resolution. This multi-line approach has the advantage of taking into account the correct line-by-line $g_{\rm eff}$ value. Leone (2007) adopted an average value, while Bagnulo et al. (2012) pointed out how the use of an average Landé factor limits the precision of the measurement of the effective magnetic field from circular polarization, because the value of $g_{\rm eff}$ varies among the lines; for many of the lines, the actual circular polarization will vary from the average by up to 25 per cent.

The process of selection started with a synthetic spectrum computed by SYNTHE (Kurucz 1993; Sbordone et al. 2004). First we removed all the lines weaker than the noise level and the lines in the region of strong lines, such as Hα and Hβ and telluric lines. The exclusion of very broad and strong spectral lines is mainly justified by the presence of line cores dominated by saturation and not by magnetic fields.

In order to select the most sensitive transitions, we included only lines whose effective Landé factor is higher than 0.7. Atomic parameters were taken from the VALD data base (Piskunov et al. 1995).

In order to find and remove blends, we evaluated the full width at half-maximum (FWHM) (in km s^{-1}) and the position of the centroid of each line through a Gaussian fit and we discarded all the transitions whose radial velocity or the FWHM was more than 3σ from the averaged value. This is possible because data were acquired with an échelle spectrograph in which $\Delta\lambda/\lambda \approx constant$. Fig. 1 shows examples of selected and unselected spectral lines. On average, a thousand spectral lines are selected for the measure.

Another possible source of error is the normalization to the continuum (Bagnulo et al. 2012). In order to limit the impact, we computed the pseudo-continuum level of each line through the linear fit of the highest 10 points in a region of 3 Å centred on the wavelength of the transition, half on the right and half on the left (Fig. 2).

For each line (with index j) we computed the quantity

$$x_{ij} = -4.67 \times 10^{-13}\ \lambda_{0j}^2\ g_{\rm eff_j}\ \frac{1}{I_{ij}(\lambda)}\ \frac{{\rm d}I_{ij}(\lambda)}{{\rm d}\lambda_{ij}}, \qquad (7)$$

where i extends over the pixels. It can be noted that equation (7) allows the use of the effective Landé factor $g_{\rm eff}$ of each particular line instead of the average value. The spectral derivative ${\rm d}I_{ij}(\lambda)/{\rm d}\lambda_{ij}$ was computed using a three-point Lagrange interpolation. Spikes in the spectra, caused by cosmic rays, for example, can affect the measurement of the magnetic field. In order to avoid this, we performed a clipping of the null profile, rejecting all V/I points whose N/I is more than 5σ from the average (Bagnulo et al. 2006).

We determined the magnetic field through minimization of χ^2, as given by

$$\chi^2 = \sum_{ij} \frac{(y_{ij} - B_{\rm eff}\ x_{ij} - b)^2}{\sigma_{ij}^2}, \qquad (8)$$

where b is a constant term related to the residual instrumental polarization (Bagnulo et al. 2002). We used $y_{ij} = V_{ij}/I_{ij}$ for the measurement of the magnetic field, and $y_{ij} = N_{ij}/I_{ij}$ for the estimation of systematic errors. This is possible because the null profile is, in principle, related to systematic errors resulting from observations or from the data-reduction procedure. Finally, the total error was given by the quadratic sum of the systematic error and the standard error of the fit. In the case of a good measurement, we expect the slope of N_{ij}/I_{ij} to be zero within the error range (Leone 2007).

Fig. 3 shows an example of the magnetic field measurements obtained with the application of the multi-line slope method to

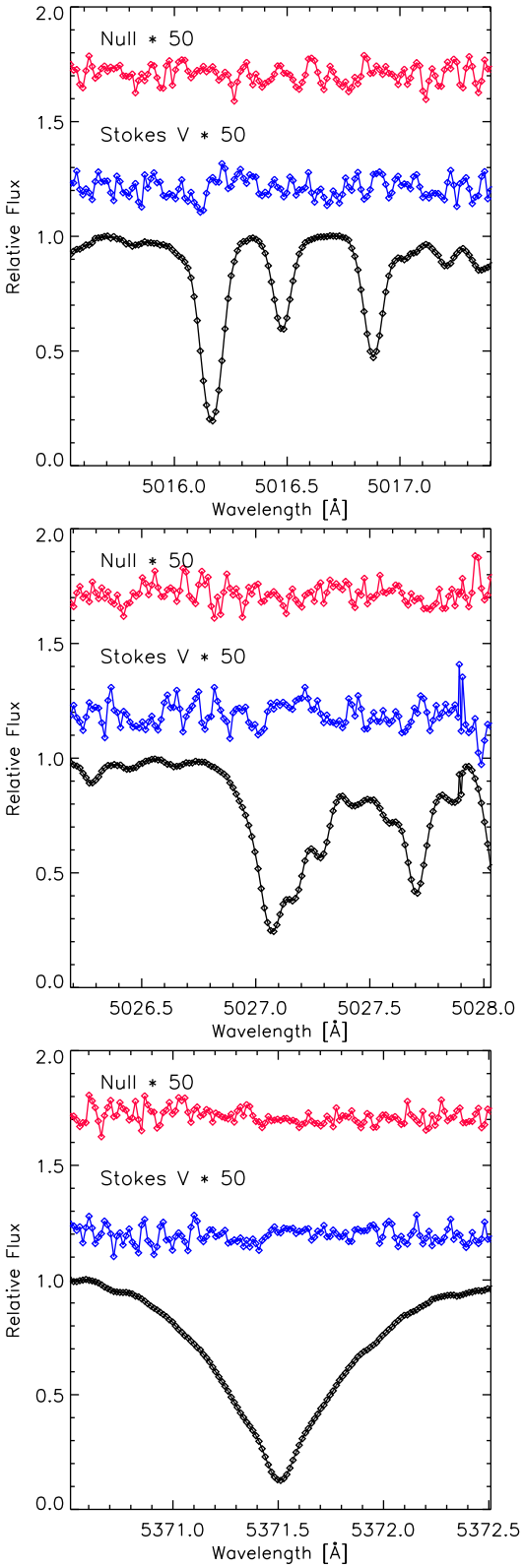

Figure 1. Examples of selections of the spectra of ϵ Eri observed with HARPSpol on 2010 January 5. From top to bottom we report examples of selected unblended lines, unselected blend lines and unselected strong lines.

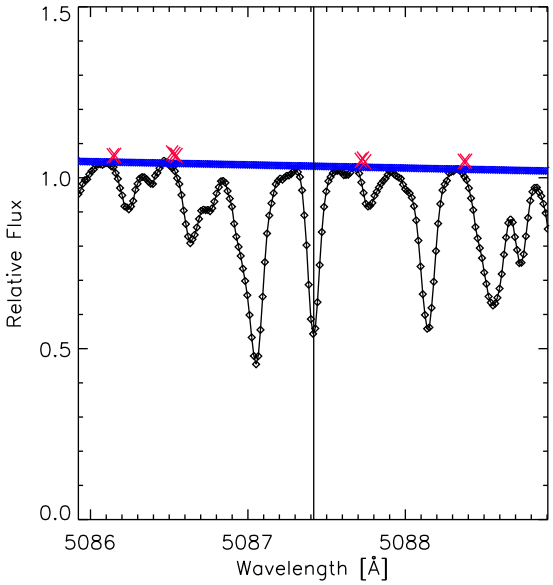

Figure 2. Example of the normalization of Stokes *I*; the linear pseudo-continuum is shown in blue, and the points used for the fit are in red.

high-resolution spectra of the cool star ϵ Eri observed by HARPSpol using a total of 3900 lines.

4.1 Numerical tests

In order to test the capabilities of the multi-line slope method we computed synthetic spectra using COSSAM (Codice per la Sintesi Spettrale nelle Atmosfere Magnetiche) (Stift, Leone & Cowley 2012). It is a fully parallelized code that solves the polarized radiative transfer equation for a stellar atmosphere permeated by a magnetic field under the assumption of local thermal equilibrium (LTE). The code calculates the emergent Stokes *IQUV* spectrum integrated over the visible stellar disc. Details of design decisions and implementation can be found in Stift & Dubois (1998) and Stift (1998).

All synthetic profiles were convolved with the respective FWHM of CAOS, NARVAL and HARPSpol and re-sampled to conform with the wavelength binnings. Simulations were performed considering a dipolar magnetic field geometry centred on the star, with $i = 135^{\circ}$ and $\beta = 50^{\circ}$, considering a zero phase.

First, we tested the effects of the rotational velocity on the measurements; the results are given in Table 1. It can be seen that for very low values of rotational velocity (lower than 5 km s^{-1}), the results of the multi-line slope method differ with respect to the input by the order of 20 per cent. This difference increases with rotational velocity, and for $v \sin i > 30$ km s^{-1} it exceeds 50 per cent. We attribute this to the large rotational velocity values, which affect the shape of the line profile and its derivative in a non-negligible way.

A second simulation tested the effects of the field strength on the measurements, in the case of low rotational velocity ($v \sin i = 3$ km s^{-1}). It can be seen from Table 2 that the multi-line slope method gives results that differ by about 20 per cent from the input value for field strengths lower than 1000 G. For values higher than 1000 G, the method underestimates the field, with the discrepancy increasing with the spectral resolution. These findings could be explained by the fact that for higher resolution and higher field values Zeeman splitting is dominant, and so the first

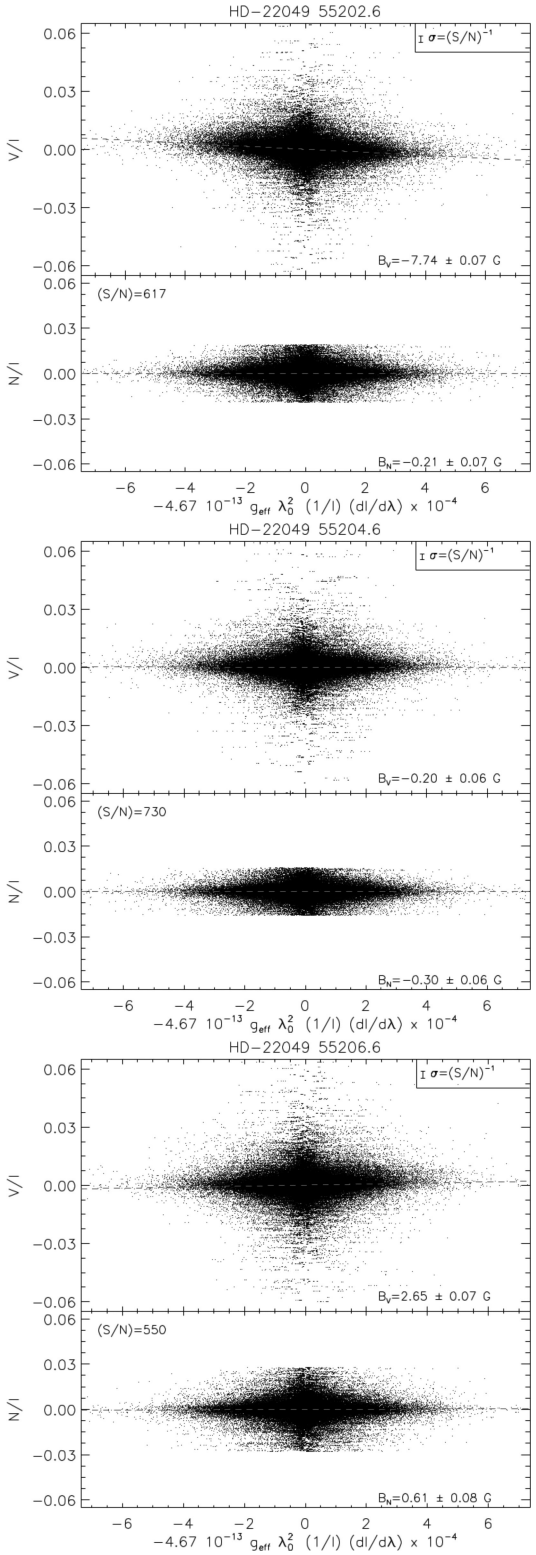

Figure 3. Magnetic field measurements of ϵ Eri from HARPSpol data. The top part of each panel shows the Stokes *V* profiles and the bottom parts show the null profiles, both as a function of the spectral derivative of Stokes *I*. The presence of the magnetic field is reflected in the slope of the distribution. The flat distribution of the null profile confirms the good quality of the measure. The panels refer, from top to bottom, to the observations made on the nights of 2010 January 5, 7 and 9. The sizes of the typical error bar are showed in the figures; the signal-to-noise ratio (S/N) is calculated from the standard deviation of the null profile's points.

Table 1. Results of effective magnetic field measurement from the multi-line slope method (B_{ms}) and from the slope method applied to all the simulated data points in the spectral region (B_{slope}) versus rotational velocity. The input effective magnetic field is $B_{inp} = -6.45$ G.

	CAOS $R = 55000$ 2.5 px per FWHM					NARVAL $R = 65000$ 2.5 px per FWHM					HARPSpol $R = 115000$ 4.1 px per FWHM				
$v \sin i$ [km s^{-1}]	B_{ms} [G]	$\Delta B_{inp\text{-}ms}$ (per cent)	Lines	B_{slope} [G]	$\Delta B_{inp\text{-}slope}$ (per cent)	B_{ms} [G]	$\Delta B_{inp\text{-}ms}$ (per cent)	Lines	B_{slope} [G]	$\Delta B_{inp\text{-}slope}$ (per cent)	B_{ms} [G]	$\Delta B_{inp\text{-}ms}$ (per cent)	Lines	B_{slope} [G]	$\Delta B_{inp\text{-}slope}$ (per cent)
0	−6.59	2	697	−8.60	33	−6.69	4	697	−8.46	31	−6.33	−2	697	−7.72	20
3	−7.28	13	688	−9.18	42	−7.21	12	688	−9.12	41	−7.08	10	688	−8.83	37
6	−8.13	26	615	−10.04	56	−8.24	28	615	−10.15	57	−8.20	27	615	−10.17	58
9	−8.49	32	537	−10.57	64	−8.66	34	537	−10.67	65	−8.57	33	537	−10.53	63
12	−8.53	32	411	−10.72	66	−8.51	32	411	−10.70	66	−8.44	31	411	−10.48	63
15	−8.74	35	301	−10.74	66	−8.69	35	301	−10.67	65	−8.50	32	301	−10.43	62
18	−8.85	37	236	−10.80	67	−8.64	34	236	−10.57	64	−8.54	32	236	−10.43	62
21	−8.99	39	187	−10.74	67	−9.08	41	187	−10.66	65	−8.80	36	187	−10.39	61
24	−9.43	46	146	−10.77	67	−9.31	44	146	−10.57	64	−9.17	42	146	−10.31	60
27	−9.29	44	104	−10.60	64	−9.40	46	104	−10.67	65	−9.23	43	104	−10.29	60
30	−9.92	54	61	−10.58	64	−10.37	61	61	−10.65	65	−10.02	55	61	−10.29	60
33	−10.79	67	48	−10.76	67	−10.31	60	48	−10.80	67	−10.25	59	48	−10.34	60

Table 2. Results of effective magnetic field measurement from the multi-line slope method (B_{ms}) and from the slope method applied to all the simulated data points in the spectral region from 500 to 600 nm (B_{slope}) versus effective magnetic field strength. The rotational velocity is $v \sin i = 3$ km s^{-1}.

	CAOS $R = 55000$ 2.5 px per FWHM					NARVAL $R = 65000$ 2.5 px per FWHM					HARPSpol $R = 115000$ 4.1 px per FWHM				
B_{inp} [G]	B_{ms} [G]	$\Delta B_{inp\text{-}ms}$ (per cent)	Lines	B_{slope} [G]	$\Delta B_{inp\text{-}slope}$ (per cent)	B_{ms} [G]	$\Delta B_{inp\text{-}ms}$ (per cent)	Lines	B_{slope} [G]	$\Delta B_{inp\text{-}slope}$ (per cent)	B_{ms} [G]	$\Delta B_{inp\text{-}ms}$ (per cent)	Lines	B_{slope} [G]	$\Delta B_{inp\text{-}slope}$ (per cent)
0.63	0.66	5	1344	0.91	43	0.72	13	1344	0.93	46	0.70	10	1344	0.89	40
6.35	7.37	16	1342	9.23	45	7.17	13	1342	9.09	43	7.07	11	1342	8.87	40
65	75	18	1348	91	44	75	18	1348	91	43	73	15	1348	88	39
635	684	8	1341	819	29	681	7	1341	815	28	649	2	1341	788	24
3175	2323	−27	675	2740	−14	2155	−32	675	2495	−21	1516	−52	675	1697	−47

derivative of Stokes I is no longer simply related to Stokes V through equation (6).

We can conclude that the assumption of small velocity broadening made in equation (6) is valid. Therefore, for very low stellar rotational velocities ($v \sin i < 5$ km s^{-1}) and low effective field strengths ($B_{eff} < 1kG$) the multi-line slope method is a valid technique for measuring the effective magnetic field.

The simulations of Tables 1 and 2 also show the advantage of the multi-line approach. Indeed, it can be seen that the technique gives results closer to the input, better than 20 per cent with respect to the slope method applied on all the simulated data points in the spectral region; this behaviour is systematic, except for high field strengths.

The first two simulations were computed without considering the effects of the degradation caused by the photon noise. The third simulation tests the capabilities of the multi-line slope method to retrieve the effective magnetic field for spectra with a finite signal-to-noise ratio.

For each point in the synthetic spectra, we generated a random number, from a normal distribution with a mean of zero and a standard deviation of one, and we divided it by the desired value of the signal-to-noise ratio and by the square root of the synthetic Stokes I. This noise η was added to the combination of Stokes profiles:

$$\begin{aligned} s_1 &= (I + V) + \eta \\ s_2 &= (I - V) + \eta, \end{aligned} \tag{9}$$

which can be used to compute the noise synthetic profiles $\widetilde{I}$ and $\widetilde{V}$ through

$$\begin{aligned} \widetilde{I} &= \frac{s_1 + s_2}{2} \\ \widetilde{V} &= \frac{s_1 - s_2}{2}. \end{aligned} \tag{10}$$

Each measure was repeated 100 times with different random numbers, in order to compute the average B_{ms} and the standard deviation σB_{ms}.

The results of Table 3 show that, for low field values, the errors and the differences between the input and results decrease at higher resolution. The simulations reveal that a minimum signal-to-noise ratio of 250 is needed in Stokes V in order to measure the effective magnetic field with an error lower than 3σ, for the CAOS resolution.

All the previous simulations were computed considering a dipolar magnetic field geometry, centred on the star. In order to test the effect of a different geometry, we performed a measure considering a more general model, using a decentred dipole (Stift 1974). The results in Table 4 show that the method can be applied also in this case, and, for this reason, we can conclude that choice of dipolar configuration does not affect the measure.

5 COMPARISON WITH THE LEAST SQUARES DECONVOLUTION TECHNIQUE

Magnetic field measurements from high-resolution spectropolarimetric data are often made using LSD. This method is based on

Table 3. Results of effective magnetic field measurement from the multi-line slope method (B_{ms}) versus the signal-to-noise ratio. The input effective magnetic field is $B_{inp} = 6.35$ G and $v \sin i = 3$ km s^{-1}. σB_{ms} is the standard deviation of the measurements in the simulation (details in the text). The spectral region is between 500 and 600 nm.

	CAOS $R = 55000$ 2.5 px per FWHM				NARVAL $R = 65000$ 2.5 px per FWHM				HARPSpol $R = 115000$ 4.1 px per FWHM			
S/N	B_{ms} [G]	σB_{ms} [G]	$\Delta B_{inp\text{-}ms}$ (per cent)	Lines	B_{ms} [G]	σB_{ms} [G]	$\Delta B_{inp\text{-}ms}$ (per cent)	Lines	B_{ms} [G]	σB_{ms} [G]	$\Delta B_{inp\text{-}ms}$ (per cent)	Lines
100	4.18	5.50	−34	1274	6.13	4.88	−3	1348	5.98	1.66	−6	1537
250	8.13	1.88	28	1310	7.34	2.21	16	1375	6.90	0.63	9	1512
500	7.18	1.62	13	1322	7.14	0.66	12	1382	6.76	0.34	6	1517
1000	7.41	0.50	17	1333	7.13	0.34	12	1389	6.92	0.18	9	1519

Table 4. Results of the effective magnetic field measurement from the multi-line slope method (B_{ms}) and from the slope method applied to all the simulated data points in a region from 500 to 550 nm (B_{slope}) in the case of the decentred dipole model for the magnetic field geometry.

	CAOS $R = 55000$ 2.5 px per FWHM					NARVAL $R = 65000$ 2.5 px per FWHM					HARPSpol $R = 115000$ 4.1 px per FWHM				
B_{inp} [G]	B_{ms} [G]	$\Delta B_{inp\text{-}ms}$ (per cent)	Lines	B_{slope} [G]	$\Delta B_{inp\text{-}slope}$ (per cent)	B_{ms} [G]	$\Delta B_{inp\text{-}ms}$ (per cent)	Lines	B_{slope} [G]	$\Delta B_{inp\text{-}slope}$ (per cent)	B_{ms} [G]	$\Delta B_{inp\text{-}ms}$ (per cent)	Lines	B_{slope} [G]	$\Delta B_{inp\text{-}slope}$ (per cent)
−1.45	−1.34	−7	350	−1.77	22	−1.34	−8	362	−1.78	23	−1.26	−13	384	−1.70	17

the assumption that all the spectral lines have the same profile and can be added linearly. The LSD method can extract an average Stokes profile that can be used for the measurement of the effective magnetic field through the first-order moment of the LSD Stokes V (Kochukhov, Makaganiuk & Piskunov 2010):

$$B_{\rm eff} = -7.145 \times 10^6 \frac{\int v\, Z^V\, {\rm d}v}{\lambda_0 \bar{g} \int Z^I\, {\rm d}v}, \quad (11)$$

where Z^V is the Stokes V LSD profile, Z^I the Stokes I LSD profile, and λ_0 and $\bar{g}$ are (arbitrary) quantities adopted for the normalization of weights of the Stokes V LSD profile.

In order to compare the results of the multi-line slope method with the LSD results, we measured the effective magnetic field of ϵ Eri from the observations of HARPSpol made in 2010 and published by Piskunov et al. (2011). The quantitative values of the LSD measurements are taken from Olander (2013). It can be seen in Fig. 4 that in general the results are in agreement; however, the multi-line slope method gives results systematically lower than the LSD measurements. The reasons for this have yet to be determined.

We conclude that the multi-line slope method can be used as an alternative technique to LSD for the measurement of the effective magnetic fields of cool stars. It has the advantage of being easier and faster to compute; however, LSD can retrieve the shape of the profile, allowing the detection of magnetic field configurations with zero average values. In principle at least, the slope method can also identify a zero average field when the V/I scatter is larger than the N/I scatter.

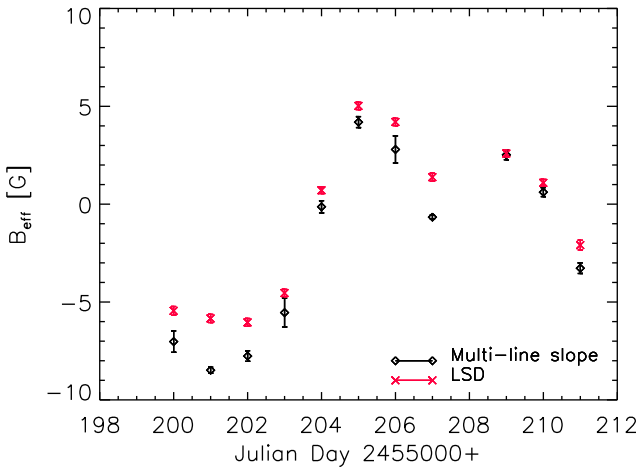

Figure 4. Comparison between the multi-line slope method (black) and LSD (red) for the ϵ Eri HARPSpol observations of 2010 January (Piskunov et al. 2011; Olander 2013).

6 THE MAGNETIC FIELD OF ϵ ERIDANI

Epsilon Eridani (HD 22049, HIP 16537) is one of the brightest and best studied solar analogues. It is a K2V star with an effective temperature of 5146 K, a mass of 0.856 $M_\odot$, and $v \sin i = 2.4$ km s^{-1} (Valenti & Fischer 2005). Infrared observations show that the star is surrounded by a debris disc (Greaves et al. 2005) with density inhomogeneities that can be explained by the existence of exoplanets (Backman et al. 2009).

In fact, though, the existence of planets in the system orbiting ϵ Eri is an open question. Hatzes et al. (2000) ascribed the long-period radial velocity (RV) variation to the presence of a planetary companion. This presence was confirmed by Benedict et al. (2006), who estimated a period $P_{\rm orbital} = 6.85 \pm 0.03$ yr and a companion mass of $M = 1.55 \pm 0.24\, M_J$. Anglada-Escudé & Butler (2012), however, concluded that the RV variability of ϵ Eri is probably caused by stellar activity cycles (not strictly periodic) rather than by the presence of a planet. The presence of a planet was not confirmed from the velocity measurements analysed by Zechmeister et al. (2013), nor from imaging (Janson et al. 2015; Mizuki et al. 2016).

The stellar activity of ϵ Eri over 45 yr was studied by Metcalfe et al. (2013), who found a short cycle of 2.95 yr modulated by a long cycle of 12.7 yr. The magnetic field could play an

Table 5. Effective magnetic field measurements of ϵEri.

MJD	$B_{\rm eff}$ [G]	Instrument	MJD	$B_{\rm eff}$ [G]	Instrument
54122.256	− 12.97 ± 0.21	NARVAL	55605.505	2.15 ± 0.25	HARPS
54127.316	7.49 ± 0.60	NARVAL	55606.504	0.72 ± 0.16	HARPS
54128.313	7.53 ± 0.31	NARVAL	55836.623	6.80 ± 0.05	NARVAL
54130.354	0.69 ± 0.26	NARVAL	55838.638	7.94 ± 0.10	NARVAL
54133.326	− 14.41 ± 0.11	NARVAL	55843.622	4.53 ± 0.14	NARVAL
54135.316	− 9.87 ± 0.18	NARVAL	55845.503	4.39 ± 0.09	NARVAL
54140.328	6.43 ± 0.12	NARVAL	55846.521	4.85 ± 0.44	NARVAL
54485.380	− 3.83 ± 0.37	NARVAL	55850.517	9.00 ± 0.12	NARVAL
54487.305	− 1.00 ± 0.06	NARVAL	55866.516	1.32 ± 0.14	NARVAL
54488.321	− 1.69 ± 0.06	NARVAL	55874.464	11.18 ± 0.12	NARVAL
54489.325	− 3.68 ± 0.21	NARVAL	55876.594	7.16 ± 0.15	NARVAL
54490.345	− 7.72 ± 0.21	NARVAL	55877.552	4.95 ± 0.13	NARVAL
54491.328	− 9.77 ± 0.33	NARVAL	55882.540	4.54 ± 0.19	NARVAL
54492.327	− 10.31 ± 0.29	NARVAL	55887.432	9.88 ± 0.08	NARVAL
54493.339	− 9.36 ± 0.08	NARVAL	56202.533	1.14 ± 0.07	NARVAL
54494.383	− 7.37 ± 0.06	NARVAL	56203.533	1.07 ± 0.23	NARVAL
54495.352	− 7.01 ± 0.08	NARVAL	56205.556	− 3.79 ± 0.17	NARVAL
54499.348	2.53 ± 0.17	NARVAL	56206.543	− 3.74 ± 0.10	NARVAL
54501.331	− 5.01 ± 0.06	NARVAL	56214.494	− 4.65 ± 0.39	NARVAL
54502.330	− 9.18 ± 0.17	NARVAL	56224.617	− 3.89 ± 0.13	NARVAL
54503.330	− 9.60 ± 0.14	NARVAL	56229.541	− 5.57 ± 0.26	NARVAL
54506.339	− 7.12 ± 0.08	NARVAL	56230.540	− 0.56 ± 0.19	NARVAL
54507.284	− 8.19 ± 0.27	NARVAL	56232.517	5.25 ± 0.07	NARVAL
54508.342	− 6.94 ± 0.07	NARVAL	56238.554	− 11.85 ± 0.14	NARVAL
54509.347	− 3.64 ± 0.20	NARVAL	56244.508	4.31 ± 0.16	NARVAL
54510.343	0.45 ± 0.29	NARVAL	56246.476	− 0.15 ± 0.38	NARVAL
54511.350	− 0.11 ± 0.07	NARVAL	56254.483	0.02 ± 0.49	NARVAL
54512.341	− 2.49 ± 0.16	NARVAL	56555.500	− 3.44 ± 0.05	NARVAL
55199.609	− 4.04 ± 0.04	HARPS	56556.500	0.56 ± 0.06	NARVAL
55200.593	− 7.02 ± 0.27	HARPS	56557.500	3.50 ± 0.23	NARVAL
55201.650	− 8.48 ± 0.08	HARPS	56575.500	− 17.29 ± 0.10	NARVAL
55202.593	− 7.74 ± 0.13	HARPS	56576.500	− 11.61 ± 0.14	NARVAL
55203.550	− 5.54 ± 0.37	HARPS	56577.500	− 4.70 ± 0.28	NARVAL
55204.569	− 0.20 ± 0.16	HARPS	56578.500	− 2.34 ± 0.13	NARVAL
55205.593	4.19 ± 0.14	HARPS	56921.608	6.02 ± 1.64	CAOS
55206.570	2.65 ± 0.35	HARPS	56922.557	5.67 ± 0.42	CAOS
55207.617	− 0.66 ± 0.06	HARPS	56922.578	4.52 ± 0.20	CAOS
55209.558	2.52 ± 0.13	HARPS	56941.499	2.12 ± 0.49	CAOS
55210.587	0.62 ± 0.11	HARPS	56946.504	− 0.36 ± 2.12	CAOS
55211.575	− 3.27 ± 0.14	HARPS	56947.504	− 3.12 ± 2.54	CAOS
55224.311	− 5.36 ± 0.08	NARVAL	56949.551	− 1.12 ± 0.16	CAOS
55231.306	− 2.42 ± 0.72	NARVAL	57044.323	4.65 ± 0.15	CAOS
55241.276	5.21 ± 0.31	NARVAL	57630.549	− 10.58 ± 1.39	CAOS
55242.271	1.78 ± 0.12	NARVAL	57630.580	− 6.10 ± 2.34	CAOS
55600.534	− 1.66 ± 0.05	HARPS	57634.617	− 6.12 ± 1.31	CAOS
55601.509	− 0.78 ± 0.09	HARPS	57723.443	− 6.41 ± 1.64	CAOS
55602.599	− 1.44 ± 0.04	HARPS	57724.413	− 9.74 ± 2.13	CAOS

important role in this star. In order to study its long-term variation, Jeffers et al. (2014) performed spectropolarimetric observations; they collected Stokes I and V profiles at six epochs in a range of 7 yr, using the spectropolarimeters NARVAL and HARPSpol. They found that the large-scale magnetic field is highly variable, with no common pattern over the years, and they concluded that more observations were needed to investigate the magnetic activity of this star.

The multi-line slope method measurements of all available high-resolution spectropolarimetric data are reported in Table 5. Fig. 5 shows the highly variable behaviour of the effective magnetic field of the star, folded with the rotational period. Note that some curves are characterized by a change of polarity of the field (Narval 2007, HARPSpol 2010 and Narval 2013); in others, the magnetic field has the same sign as in the case of NARVAL 2011. Sinusoidal fits, shown in Fig. 5, are obtained using

$$f(t) = A_0 + A_1 \sin\left(2\pi \frac{t - t_0}{P} + A_2\right) + A_3 \sin\left(4\pi \frac{t - t_0}{P} + A_4\right), \quad (12)$$

where t is the time in days, t_0 is a reference time equal to MJD 54101 (Jeffers et al. 2014), P is the variability period assumed as

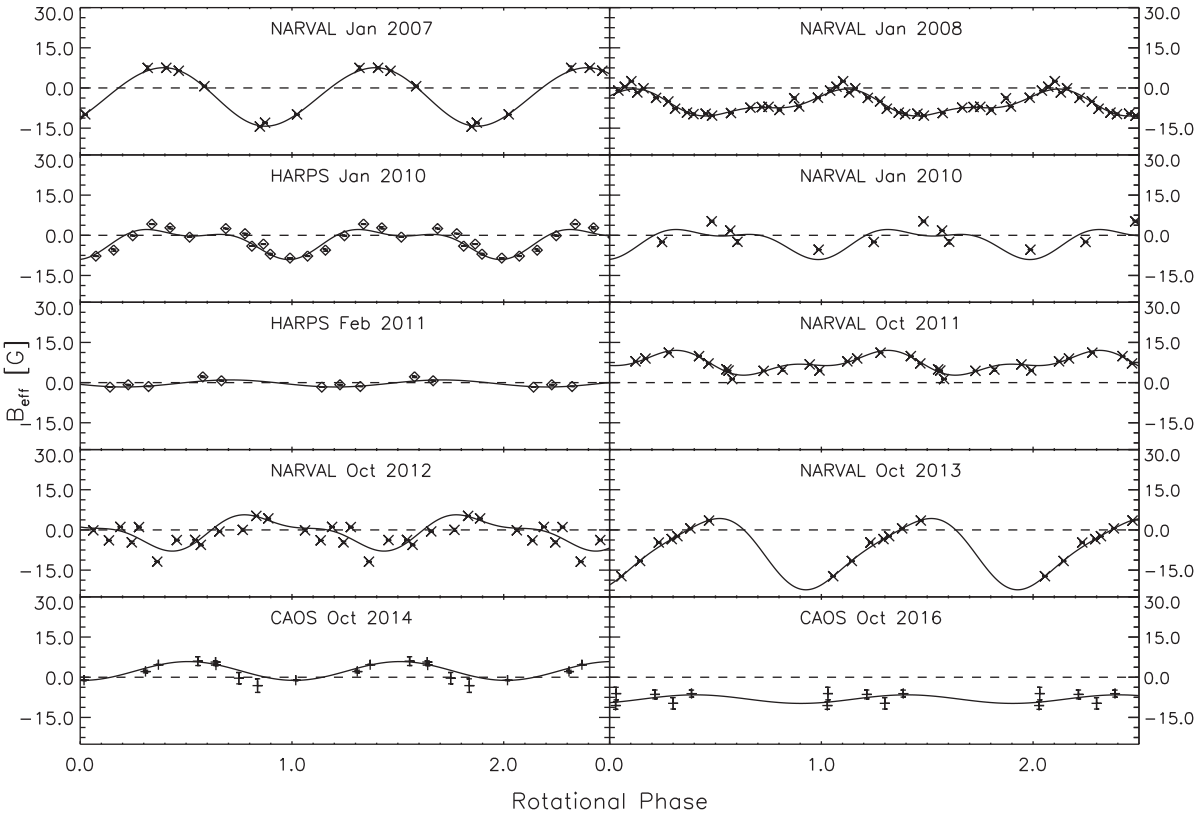

Figure 5. Magnetic curves of ϵ Eri folded with the period of rotation of the star, $P_{\rm rot} = 11.35$ d (Fröhlich 2007). Cross, diamonds and pluses refer to observations obtained respectively with NARVAL, HARPSpol and CAOS. Zero phase is equal to MJD 54101 (Jeffers et al. 2014). Magnetic curves are obtained by a fitting through equation (12) (see text).

the rotational one, A_1 and A_3 are amplitudes (expressed in gauss), A_2 and A_4 are phase shifts, and A_0 represents the level of the variation of the curves (in gauss). The fits of the data of CAOS and HARPS 2011 were obtained using a single wave ($A_3 = A_4 = 0$) because of the low number of measured points in their magnetic curves, and the magnetic curve of 2010 January was obtained using both HARPSpol and NARVAL data.

In order to find periodicities in the effective magnetic field we computed the Fourier transform following Deeming (1975). We deconvolved in the frequency domain using the CLEAN algorithm (Roberts, Lehar & Dreher 1987) in order to limit the effects of artefacts caused by the incompleteness of the sampling. The results are reported in Fig. 6. Fitting a Gaussian, we estimated the position of the main peaks at $P_1 = 976 \pm 70$ d and $P_2 = 555 \pm 22$ d; errors are assumed to be as large as the FWHM of the Gaussian. Note that P_1 is close to the 2.95-yr period found by Metcalfe et al. (2013) (Fig. 7). Indeed, the period corresponds to that found by Lehmann et al. (2015) by analysing the magnetic field from the Zeeman broadening.

Another analysis can be performed on the variation of the level of the curves A_0. This is done in order to separate the short-term sinusoidal variations – resulting from stellar rotation – from long-term changes in the constant term A_0, obtained by equation (12). The values of A_0 are reported in Table 6, with the average time of the magnetic curves. The Fourier transform (Fig. 8) exhibits periods close to those of the effective magnetic field at $P_1 = 1099 \pm 71$ d and $P_2 = 517 \pm 17$ d. In order to find the best period we computed χ^2 for a sinusoidal fit to the A_0 values, folded with the two periods. The results, reported in the bottom panel of Fig. 8, reveal that P_1 is the best period.

7 CONCLUSIONS

We have introduced an extension to a method developed by Bagnulo et al. (2002) for measuring the effective magnetic field of stars from low-resolution spectropolarimetry by means of a regression of Stokes V against the spectral derivative of Stokes I. Our multi-line slope method, based on high-resolution spectropolarimetry, instead uses similar information from the Stokes profiles of a large number of unblended lines. We carried out tests of the new method, using the polarized radiative transfer code COSSAM, concluding that the results are satisfactory for stars with low rotational velocities ($v \sin i < 5$ km s^{-1}) and field strengths ($B_{\rm eff} < 1$ kG).

The comparison with the popular LSD shows that the multi-line slope method can be an easy-to-use and fast alternative for measuring the effective magnetic field of late-type stars. LSD, however, offers the advantage of retrieving the shape of the Stokes profile; this makes it possible to infer the presence of a magnetic field with zero average value.

Finally, we applied the technique to all the available spectropolarimetric data of the star ϵ Eri. We separated the short-term variation of the effective magnetic field, resulting from stellar rotation, from the long-term variation through the coefficient A_0 (defined in equation 12); we used a Fourier transform to discover that the best-fitting period of the variation of A_0 ($P_1 = 1099 \pm 71$ d) is close to the short cycle period in the S-index found by Metcalfe et al.

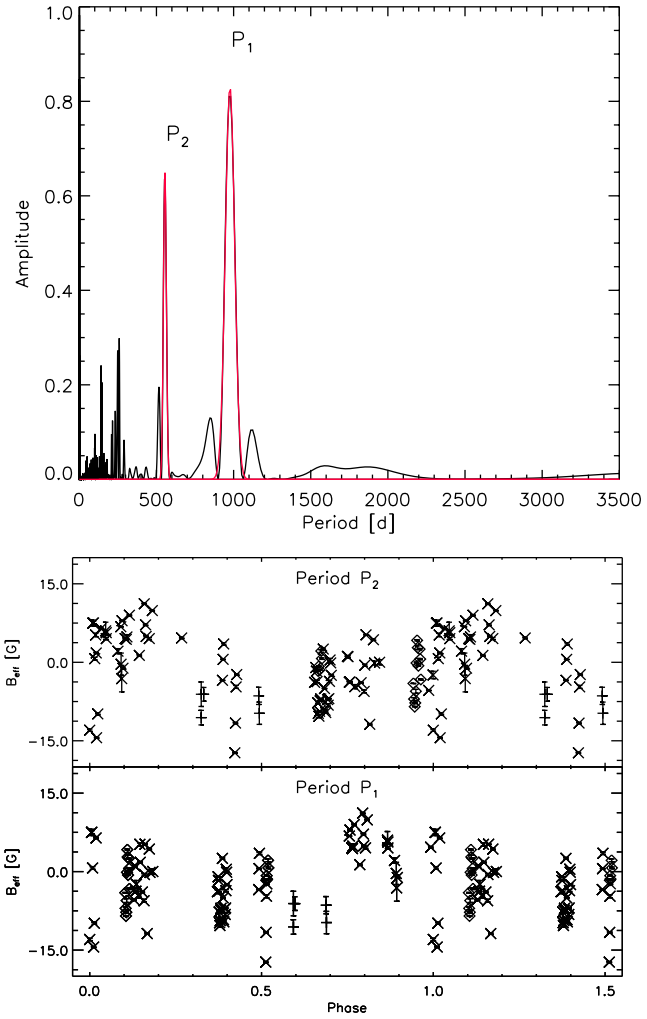

Figure 6. Top: Cleaned Fourier transform of the effective magnetic field of ϵ Eri (black) (Deeming 1975; Roberts et al. 1987) and Gaussian fit of the main periods (red). Bottom: Effective magnetic field measurements (Table 5) folded with the two periods. Crosses, diamonds and pluses refer to observations obtained respectively with NARVAL, HARPSpol and CAOS.

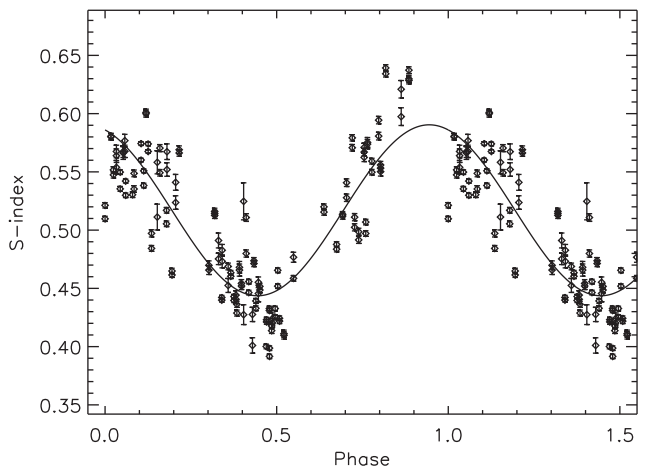

Figure 7. S-index measurements (Metcalfe et al. 2013) folded with the period P_1.

Table 6. Table of the values of A_0.

$MJD_{average}$	A_0 [G]
54131.030	− 3.15 ± 0.21
54498.337	− 6.08 ± 0.03
55205.339	− 2.19 ± 0.04
55603.330	− 0.31 ± 0.04
55860.543	7.12 ± 0.03
56225.684	− 0.58 ± 0.04
56568.214	− 8.27 ± 0.67
56949.516	2.34 ± 0.67
57668.720	− 8.17 ± 0.67

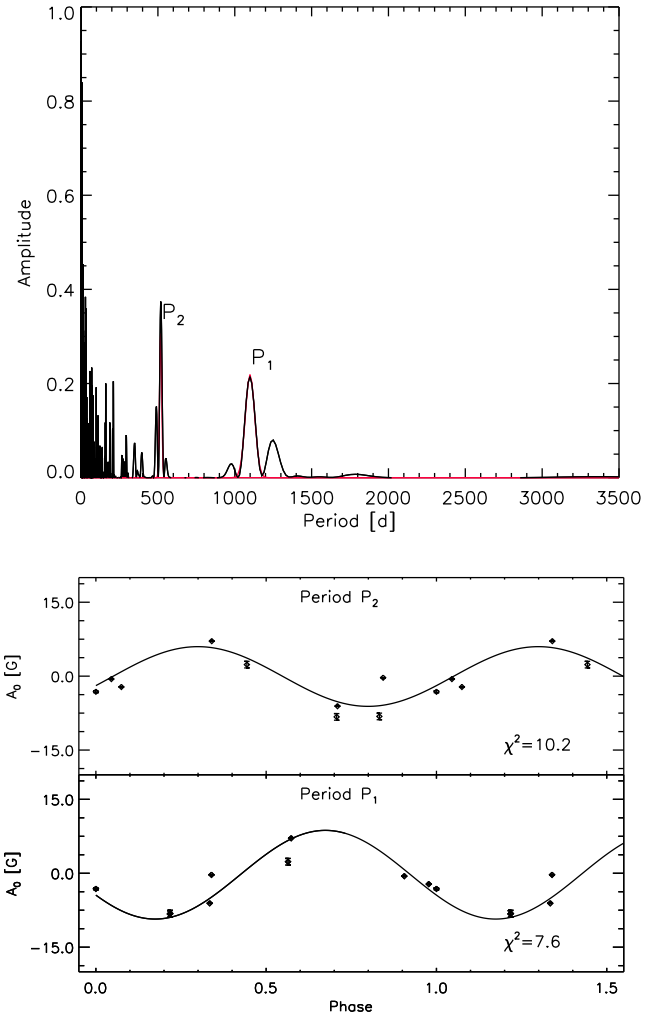

Figure 8. Top: Cleaned Fourier transform of A_0 (black) (Deeming 1975; Roberts et al. 1987) and Gaussian fit of the main periods (red). Bottom: A_0 folded with the two periods.

(2013) and to the period of the magnetic field found by an analysis of the Zeeman broadening (Lehmann et al. 2015). Direct measurements of the effective magnetic field thus open up the possibility of determining the periods of the cycles of active cool stars.

ACKNOWLEDGEMENTS

This research is based on observations collected at the European Organization for Astronomical Research in the Southern Hemisphere

under ESO programmes 084.D-0338(A) and 086.D-0240(A). This research has used the PolarBase data base.

REFERENCES

Anglada-Escudé G., Butler R. P., 2012, ApJS, 200, 15
Aurière M., 2003, in Arnaud J., Meunier N., eds, ESA SP-9, Magnetism and Activity of the Sun and Stars. ESA, Noordwijk, p. 105
Backman D. et al., 2009, ApJ, 690, 1522
Bagnulo S., Szeifert T., Wade G. A., Landstreet J. D., Mathys G., 2002, A&A, 389, 191
Bagnulo S., Landstreet J. D., Mason E., Andretta V., Silaj J., Wade G. A., 2006, A&A, 450, 777
Bagnulo S., Landstreet J. D., Fossati L., Kochukhov O., 2012, A&A, 538, 129
Benedict G. F. et al., 2006, AJ, 132, 2206
Bouvier J. et al., 2007, A&A, 463, 1017
Carolo E. et al., 2014, A&A, 567, 48
Deeming T. J., 1975, Ap&SS, 36, 137
Desidera S. et al., 2004, A&A, 420, L27
Donati J.-F., Semel M., Carter B. D., Rees D. E., Collier Cameron A., 1997, MNRAS, 291, 658
Dumusque X. et al., 2012, Nature, 491, 207
Fröhlich H.-E., 2007, Astronomische Nachrichten, 328, 1037
Greaves J. S. et al., 2005, ApJ, 619, L187
Hatzes A. P. et al., 2000, ApJ, 544, L145
Hubrig S., Scholz K., Hamann W.-R., Schöller M., Ignace R., Ilyin I., Gayley K. G., Oskinova L. M., 2016, MNRAS, 458, 3381
Janson M., Quanz S. P., Carson J. C., Thalmann C., Lafrenière D., Amara A., 2015, A&A, 574, 120
Jeffers S. V., Petit P., Marsden S. C., Morin J., Donati J.-F., Folsom C. P., 2014, A&A, 569, 79
Judge P. G., Thompson M. J., 2012, in Mandrini C. H., Webb D. F., eds, Proc. IAU Symp. 286, Comparative Magnetic Minima: Characterizing Quiet Times in the Sun and Stars. Kluwer, Dordrecht, p. 15 (doi:10.1017/S1743921312004589)
Kane S. R. et al., 2016, ApJ, 820, L5
Kochukhov O., Makaganiuk V., Piskunov N., 2010, A&A, 524, 5
Kolenberg K., Bagnulo S., 2009, A&A, 498, 543
Kurucz R. L., 1993, SYNTHE spectrum synthesis programs and line data. Smithsonian Astrophysical Observatory, Cambridge, MA [CD-ROM]
Landstreet J. D., 1982, ApJ, 258, 639
Lehmann L. T., Künstler A., Carroll T. A., Strassmeier K. G., 2015, Astronomische Nachrichten, 336, 258
Leone F., 2007, MNRAS, 382, 1690
Leone F., Martínez González M. J., Corradi R. L. M., Privitera G., Manso Sainz R., 2011, ApJ, 731, L33
Leone F. et al., 2016, AJ, 151, 116
Metcalfe T. S. et al., 2013, ApJ, 763, L26
Mizuki T. et al., 2016, A&A, 595, 79
Morgenthaler A. et al., 2010, in Boissier S., Heydari-Malayeri M., Samadi R., Valls-Gabaud D., eds, SF2A-2010: Proc. Annual Meeting of the French Society of Astronomy and Astrophysics. p. 269
Olander T., 2013, The magnetic field of ϵ Eri. Available at: http://www.diva-portal.org/smash/record.jsf?pid=diva2%3A627839&dswid=4955
Petit P., Louge T., Théado S., Paletou F., Manset N., Morin J., Marsden S. C., Jeffers S. V., 2014, PASP, 126, 469
Pevtsov A. A., Fisher G. H., Acton L. W., Longcope D. W., Johns-Krull C. M., Kankelborg C. C., Metcalf T. R., 2003, ApJ, 598, 1387
Piskunov N. E., Kupka F., Ryabchikova T. A., Weiss W. W., Jeffery C. S., 1995, A&AS, 112, 525
Piskunov N. et al., 2011, The Messenger, 143, 7
Preusse S., Kopp A., Büchner J., Motschmann U., 2006, A&A, 460, 317
Queloz D. et al., 2001, A&A, 379, 279
Reiners A., 2012, Living Rev. Sol. Phys., 9, 1
Roberts D. H., Lehar J., Dreher J. W., 1987, AJ, 93, 968
Sbordone L., Bonifacio P., Castelli F., Kurucz R. L., 2004, Memorie della Societa Astronomica Italiana Supplementi, 5, 93
Schrijver C. J., Cote J., Zwaan C., Saar S. H., 1989, ApJ, 337, 964
Semel M., Li J., 1996, Sol. Phys., 164, 417
Semel M., Ramírez Vélez J. C., Martínez González M. J., Asensio Ramos A., Stift M. J., López Ariste A., Leone F., 2009, A&A, 504, 1003
Sennhauser C., Berdyugina S. V., 2010, A&A, 522, 57
Snik F. et al., 2011, in Kuhn J. R., Harrington D. M., Lin H., Berdyugina S. V., Trujillo-Bueno J., Keil S. L., Rimmele T., eds, Astronomical Society of the Pacific Conference Series Vol. 437, Solar Polarization 6. Astron. Soc. pac., San Francisco, p. 237
Stift M. J., 1974, MNRAS, 169, 471
Stift M. J., 1998, (Astro)physical supercomputing: Ada95 as a Safe, Object Oriented Alternative. Springer, Berlin, pp. 128–139 (doi:10.1007/BFb0055000). Available at: http://dx.doi.org/10.1007/BFb0055000
Stift M. J., Dubois P. F., 1998, Comput. Phys., 12, 150
Stift M. J., Leone F., Cowley C. R., 2012, MNRAS, 419, 2912
Strugarek A., Brun A. S., Matt S. P., Réville V., 2015, ApJ, 815, 111
Tinbergen J., Rutten R., 1992, WHT Spectropolarimetry user manual. Available at: https://www.ing.iac.es/Astronomy/observing/manuals/html_manuals/wht_instr/isispol/isispol.html
Unno W., 1956, PASJ, 8, 108
Valenti J. A., Fischer D. A., 2005, ApJS, 159, 141
Zechmeister M. et al., 2013, A&A, 552, 78

This paper has been typeset from a TEX/LATEX file prepared by the author.